Object-Based Cognitive Map in the Human Hippocampus and Medial Prefrontal Cortex

Authors: Bo Zhang[1] and Yuji Naya[1, 2, 3, 4, 5, *]

Affiliations:

[1] School of Psychological and Cognitive Sciences, Peking University, No. 52, Haidian Road, Haidian District, Beijing 100805, China

[2] Center for Life Sciences, Peking University, No. 52, Haidian Road, Haidian District, Beijing 100805, China

[3] IDG/McGovern Institute for Brain Research at Peking University, No. 52, Haidian Road, Haidian District, Beijing 100805, China

[4] Beijing Key Laboratory of Behavior and Mental Health, Peking University, No. 52, Haidian Road, Haidian District, Beijing 100805, China

[5] Lead contact

Contact Info: *Correspondence: yujin@pku.edu.cn

Summary

A cognitive map, representing an environment around oneself, is necessary for spatial navigation. However, compared with its constituent elements such as individual landmarks, neural substrates of coherent spatial information remain largely unknown. The present study investigated how the brain codes map-like representations in a virtual environment specified by the relative positions of three objects. Representational similarity analysis revealed an object-based spatial representation in the hippocampus (HPC) when participants located themselves within the environment, while the medial prefrontal cortex (mPFC) represented it when they recollected a target object's location relative to their self-body. During recollection, task-dependent functional connectivity increased between the two areas implying exchange of self- and target-location signals between HPC and mPFC. Together, the coherent cognitive map, which could be formed by objects, may be recruited in HPC and mPFC for complementary functions during navigation, which may generalize to other aspects of cognition, such as navigating social interactions.

Key words: cognitive map, spatial navigation, episodic memory, memory-guided decision making, social interaction, hippocampus, medial prefrontal cortex, default-mode network, representational similarity analysis.

Introduction

During navigation, it is necessary to locate our self-position in the current spatial environment as well as to locate the objects relative to the self-body (i.e., egocentric location). To conduct each of the two mental operations, we need map-like representations, called "cognitive map" in our brain (Tolman, 1948). After the discovery of "place cells," the hippocampus (HPC) of the medial temporal lobe (MTL) has been considered responsible for the cognitive map (Buffalo, 2015), and crucial contributions of the HPC to spatial memory have also been reported by animal model studies that evaluated behavioral patterns of rodents with an inactivated HPC using the Morris water maze and cross-maze (Nakazawa et al., 2002; Packard and McGaugh, 1996; Redish and Touretzky, 1998) as well as human studies that demonstrated the relationship between HPC volume in individual subjects and their amounts of experience exploring spatial environments (Woollett and Maguire, 2011; Schinazi et al., 2013, e.g., London taxi drivers). However, it remains largely unknown how neural substrates of the cognitive map are involved in the two mental operations required to locate specific objects within the environment. One possible reason for the difficulty in addressing this question is that despite extensive studies on the spatial elements related to the cognitive map (e.g., self-location, head-direction etc.) (O'Keefe and Dostrovsky, 1971; Vass and Epstein, 2013; Chadwick et al., 2015; Buffalo, 2015; McCormick et al., 2018;), there is still a lack of sufficient isolation and characterization of the neural signal of the cognitive map under the previous research paradigms.

In addition to the HPC, the role of the medial prefrontal cortex (mPFC) in goal-directed planning during navigation was demonstrated by a previous human fMRI study that showed increased connectivity between the HPC and mPFC (Brown et al., 2016). The mPFC has been long considered as a member of the core-brain system in the retrieval of episodic memory (Konishi et al., 2000; Eichenbaum, 2017; McCormick et al., 2018), which is an

autobiographical memory consisting of spatial, object, and temporal information (Suzuki and Naya, 2011; Naya and Suzuki, 2011; Squire and Wixted, 2011). Schacter et al. (2007) suggested an involvement of the mPFC in future-simulation processing and recollection of past episodes, which depend on mnemonic information stored as declarative memory including both episodic and semantic memory. Recently, they also showed increased connectivity between the HPC and mPFC during future simulation (Campbell et al., 2018). This preceding literature suggests that the HPC and mPFC, which belong to the default-mode network, work together when remembering stored information (e.g., cognitive map) and construct the mental representation of goal-directed information (e.g., target-location) from mnemonic information with the current context (e.g., self-location) (Schacter, 2012). However, the specific functional role of each of HPC and mPFC during the construction process (McCormick et al., 2018; Campbell et al., 2018) remain elusive, presumably because the construction of goal-directed information (e.g., spatial navigation) includes at least two mental operations described above (locating the self and locating an object target relative to self-location), as previous experimental paradigms did not dissociate these aspects of behavior.

To address these issues, we aimed to devise a novel 3D spatial-memory task with spatial environments defined by objects, which would enable us to identify the representation of the cognitive map and to investigate how it is related to the two mental operations (Fig. 1). We used a stimulus set consisting of three different human characters throughout the entire experiment, while the spatial configuration of the three characters was changed in a trial-by-trial manner. The spatial configuration pattern was referred to as a *"map"* in the present study (Fig. 1b). In each trial, participants encoded a *map* from the first-person's view by walking toward the characters in one of four fixed walking directions (walking period, Fig. 1c, see Methods). Following the walking period, one human character (facing object) was

presented on a virtual-environment background with other characters being invisible**,** which gave the participants a feeling of facing the presented character in the virtual environment (i.e., facing period). After a short delay, one of the two remaining characters (targeting object) was presented without the virtual environment background, and the participants were required to remember the location of this second human character relative to their self-body (i.e., targeting period). Thus, the two mental operations were separated into two periods within a single trial. This task design allowed us to detect the brain regions that distinguished the spatial configurations of the objects (i.e., *map*) around the participants during the facing period and targeting period separately. The results of the representational similarity analysis (RSA; see Methods for details) (Kriegeskorte et al., 2012; Kriegeskorte et al., 2008) showed that the spatial environment defined by the three objects were represented in the HPC during the facing period, while it was represented in the mPFC during the targeting period, suggesting different contributions of the object-based cognitive map to the recollection between the two brain areas of the default-mode network.

Results

The experiment was conducted over two days with 19 participants. On the first day, the participants were familiarized with the 3D virtual environment and the three human characters through a head-nodding detection (HND) task (Fig. S1a). In this task, the participants had the same walking experience as in the spatial-memory task but were subsequently asked to indicate whether one of the three characters in a photo had nodded its head during the walking period. On the second day, the participants performed the spatial-memory task during fMRI scanning (Fig. 1a). To prevent voluntary memorization of the spatial relationship of the human characters during the walking period, the HND trials were pseudo-randomly mixed with the spatial-memory trials at the ratio of 1:10, and the participants were instructed to focus on head-nodding of the human characters during the walking period in all trials. In each trial, its trial-type (i.e., HND or memory task) became distinguishable after the walking period by subsequent stimuli. All participants exhibited ceiling performance with a 93.6% ± 0.02% correct rate (mean ± SE, n = 19) for the spatial-memory task and no significant difference was found among each of the task parameters (e.g., maps, walking directions) (Fig. S1c). All participants also showed accuracy that was significantly higher than chance level (50%) in both the head-nodding and no head-nodding trials in the HND task (Fig. S1a). Attempts to memorize the spatial arrangements of the human characters during scanning were examined using post-scanning questionnaires. All participants reported that they did not make any voluntary effort to memorize the spatial relationship of the three human characters nor utilize any special strategy for memorizing it (Table S2). It should be noted that no participant was able to recall the number of map patterns they experienced in the experiment even though only three of the six possible patterns of maps were repeatedly presented to each participant. In addition, no significant changes in performance was found across four experimental sessions (Fig. S1b; $F(3,72) =$

0.38, P = 0.76), suggesting that the participants performed the spatial-memory task with high-performance from the beginning and did not learn to use a systematic strategy to improve their performance during the sessions. These behavioral results guarantee that the participants automatically encoded maps during the walking period when viewing the human characters attentively to detect head-nodding.

Neural representation of the cognitive map during locating self-position

We first assessed the map representation during the facing period (4.0 s including the subsequent delay; Fig. 2a), in which the participants oriented themselves to a presented human character in the 3D environment. To decode the map information across the whole brain, we conducted searchlight-based RSA, which compared the multi-voxel pattern similarities of the "same map" and "different map" between trial pairs across each brain voxel by drawing a 6 mm radius sphere with each voxel in the spherical center. Map information was decoded regardless of other task parameters such as the walking direction or the identity of the facing character by balancing the number of trials with other task parameters across the same and different map conditions during the scanning as well as excluding the effects of other task parameters in the regression analysis (see Methods for details and Table S1 for the regressor list and the averaged r^2 among the regressors in each GLM). We found a cluster located in the left middle HPC (mHPC; Fig. 2b, $P < 0.01$, voxel-wise threshold; $P < 0.05$, cluster-corrected for multiple comparison), suggesting that the map defined by multiple objects is represented in the HPC. In addition to the mHPC, the searchlight-based RSA revealed clusters in the insula, angular gyrus, and superior temporal cortex (Fig. S2b, $P < 0.01$, voxel-wise threshold; $P < 0.05$, cluster-corrected for multiple comparison; see discussion). To validate the searchlight-based RSA result showing that the left mHPC represents map information, we manually segmented the sub-regions in the MTL

in each participant's native space (Fig. S4a, top panel) and conducted an independent RSA within each anatomical mask (see Methods for details). The region of interest (ROI)-based result also showed that only the left mHPC had a significantly higher pattern similarity to "same maps" relative to "different maps" among the MTL sub-regions (Fig. S5a; $t(18) = 3.26$, $P = 0.002$, Bonferroni corrected for multiple comparisons, alpha < 0.05).

To examine possible signal input from the MTL sub-regions to the left mHPC for the map construction, we examined the neural representation of the facing-character identity and walking direction that the participants perceptually and/or mentally re-experienced during the facing period based on the post-scanning test (Table S2; Fig. S3a). Searchlight-based RSA revealed that the bilateral perirhinal cortex (PRC) encoded character identity (Fig. S3b; $P < 0.001$, initial threshold; $P < 0.05$, cluster-corrected for multiple comparison) (Naya et al., 2001; Suzuki and Naya, 2014), while the parahippocampal cortex (PHC) and left retrosplenial cortex (RSC) encoded the walking directions reflecting the spatial layout of one empty and three occupied positions perceived by the participants during the walking period (Fig. 1c). In the HPC, the left posterior HPC (pHPC) selectively represented the spatial layout but not the character identity, while the bilateral anterior HPC (aHPC) revealed clusters for both character identity and spatial layout (Fig. S3b). These results were consistent with the notion of the "two cortical systems" model suggesting that object identity and spatiotemporal context are processed in two separate neural systems with the PRC and PHC-RSC as the core brain regions, with the two different information domains interacting in the HPC (Ranganath and Ritchey., 2012). Together, the RSA analyses suggest that the MTL is associated with representing the spatial environment in the following ways**:** elements such as each object identity and spatial layout are represented by extrahippocampal areas while the relative relationship between multi-objects is represented in the HPC, suggesting cognitive map representation in the HPC.

176

177 **Cognitive map during localizing target**

178 In contrast to locate self-position, a clear difference was found in brain regions responsible
179 for the map representations when the participants remembered the location of a target
180 character relative to their self-body (egocentric target location). In contrast to the facing
181 period, clusters representing the map information were revealed mainly in the Rectus and
182 Brodmann area 10 of the mPFC (Peak coordinates: 4, 50, -18; t value: 5.62), rather than in
183 the HPC, during the targeting period. We confirmed that no cluster was found in the MTL
184 even though a more liberal threshold was used ($P < 0.01$, voxel-wise threshold, uncorrected).
185 To validate this result, we conducted an independent RSA using frontal sub-regions of the
186 automated anatomical labeling (AAL, Fig. S4a, bottom panel) template as well as manually
187 segmented MTL sub-regions as ROIs. The result confirmed that the map information was
188 represented in the rectus of the prefrontal region (Fig. S5a, left: $t(18) = 3.67$, $P = 0.0008$,
189 right: $t(18) = 4.49$, $P = 0.0001$, Bonferroni corrected for multiple comparisons, alpha < 0.05),
190 while no MTL sub-regions including the left mHPC revealed map representation significantly
191 during the targeting period. Together with the facing period results, these results revealed a
192 double dissociation of the HPC and mPFC function in the map representation between the
193 task demands, implying that the mPFC, rather than the HPC, carried the map information
194 during the generation of the egocentric location signal of a target character. Our results
195 indicate that the HPC and mPFC may operate in a complementary manner, supporting the
196 notion of the "parallel, but interactive cognitive map" between the two brain structures
197 (Wikenheiser and Schoenbaum., 2016). Outside of the mPFC, we found clusters in the
198 precuneus and middle temporal gyrus, and the inferior frontal cortex (Fig. 2c, Fig. S2c; $P <$
199 0.001, voxel-wise threshold; $P < 0.05$, cluster-corrected for multiple comparison). These
200 three brain regions have been consistently reported to be involved in scene construction

during recalling of past experience and imagination of new experiences (Hassabis and Maguire, 2007; Bird et al., 2010; Gaesser et al., 2013), which is consistent with the post-scanning report showing that all participants recalled and also imagined the egocentric positions of the three human characters during the targeting period.

As with the facing period, we examined neural representation of targeting character identity and walking direction during the targeting period and found that the PRC stably represented character identity (Fig. S3b; $P < 0.001$, initial threshold; $P < 0.05$, cluster-corrected for multiple comparison), while we did not find clusters for the spatial layout depending on the walking direction in the MTL. These results suggested that the HPC did not construct the map information from its constituent elements during the targeting period.

Current self-orientation on the map

To compute the egocentric location of a target object (e.g., left, right, or back), information on the current self-position/orientation on the map is necessary (Fig. 3a). Therefore, we examined which brain regions were involved in representing such allocentric "heading-direction" signals (Hargreaves et al., 2005; Wang et al., 2018). Interestingly, while no significant cluster was revealed during the facing period (facing character; Fig. 3b and Supplementary Fig. S5b), robust clusters were revealed during the targeting period (Fig. 3b, $P < 0.001$, voxel-wise threshold; $P < 0.05$, cluster-corrected for multiple comparison). These clusters were located in the left ERC, bilateral HPC and PHC inside the MTL as well as in the lateral occipital cortex, parietal cortex, precuneus, and anterior cingulate cortex outside the MTL (Fig. 3b, $P < 0.001$, voxel-wise threshold; $P < 0.05$, cluster-corrected for multiple comparison). These results suggested that a self-orientation signal was induced during the targeting period, presumably because of the necessity to compute the egocentric target

location. This interpretation is consistent with the post-scanning report in which participants reported imagining their self-orientation on the map only during the targeting period.

Remembering the egocentric location of a target object

Next, we examined which brain regions signaled the egocentric location (left, right, or back relative to self-body) of a target object (Fig. 4a). The results revealed robust clusters in both the mPFC and MTL (Fig. 4a, $P < 0.001$, voxel-wise threshold; $P < 0.05$, cluster-corrected for multiple comparison). In the mPFC, we identified the rectus, medial/superior orbitofrontal cortex, and olfactory cortex. In the MTL, clusters were found in the anterior HPC. Apart from the mPFC and MTL, clusters were also found in the lateral occipital cortex, inferior parietal cortex, anterior temporal lobe, premotor cortex, and lPFC (middle and superior PFC). We also found clusters in the precuneus and posterior parietal cortex, which were previously reported to represent the egocentric location (Chadwick et al., 2015). The widely distributed clusters may indicate that the brain regions representing the egocentric target locations can be involved in either generation of the egocentric-target-location information from multiple pieces of information (cognitive map, self-orientation, and target character identity) or its maintenance while preparing for the following response. These distinct functions might be supported by three different large-scale brain networks: the dorsal attention network, frontoparietal control network, and default-mode network (Spreng and Schacter., 2011). In contrast to the robust signal observed across different brain networks for egocentric target-location, no cluster was revealed for allocentric target location relative to the spatial layout of the characters (Fig. 4b, $P < 0.001$, voxel-wise threshold; $P < 0.05$, cluster-corrected for multiple comparison), which implies that the target location may be directly retrieved in the form of egocentric coordinates rather than via its allocentric representation.

Increased default-mode network connectivity while locating a target compared with self-locating

The present results showed that the MTL and mPFC signaled a coherent map coding a spatial relationship of the three human characters during the different time periods in which different task demands were required (i.e., self-locating and target-locating). In addition, the MTL and mPFC signaled the different location information even during the same targeting period; MTL areas tended to represent allocentric self-location while the mPFC tended to represent egocentric target location. To investigate how the different functional contributions of the MTL and mPFC were substantiated by whole brain large-scale networks, we conducted a task-based functional connectivity analysis using MTL and mPFC sub-regions as seeds (six and four, respectively). For each seed, the mean regional bold signals associated with two TRs in each of facing and targeting period were estimated in each trial, and concatenated across trials to make its task-based time course, which contains 72 time points (i.e., 2 TRs × 36 trials) in each session. The task-based time course of the regional signal for each seed was correlated with each voxel's time course outside the seed and then was averaged across the four sessions for each participant, generating seed-based connectivity maps for each of facing and targeting periods (Ranganath et al., 2005). Then, we compared the connectivity between the two periods across the participants using a permutation test (see Methods for details).

First, we examined the connectivity between the MTL and mPFC subregions for each of task demands, the result indicated a significantly larger connectivity between the medial orbital frontal cortex and the MTL subregions in the targeting period relative to the facing period. (aHPC: $t(18)=4.75$, $P<0.001$, pHPC: $t(18)=3.96$, $P<0.001$, PHC: $t(18)=6.85$, $P<0.001$, Bonferroni corrected for multiple comparison, $alpha<0.05$). In addition, both the MTL and mPFC showed significantly larger connectivity to other brain areas that belong to the default-mode network and those to the dorsal attention network during the targeting period compared

to the facing period (Fig. 5b, $P < 0.01$, voxel-wise threshold; $P < 0.05$, cluster-corrected for multiple comparison). By contrast, both the MTL and mPFC showed significantly larger connectivity to the frontoparietal control network during the facing period relative to the targeting period (Fig. 5a, $P < 0.001$, voxel-wise threshold; $P < 0.05$, cluster-corrected for multiple comparison). These results suggest that both the MTL and mPFC changed their connectivity to the three functional networks across the two task periods. We next evaluated the task-based functional connectivity during each task period based on the three functional network masks (Fig. S4b, Fig. 5a, b, and see method for details). This ROI analysis revealed that the default-mode network was positively correlated with the MTL ($t(18) = 7.98$ for average across the sub-regions within MTL, $P < 0.001$) and mPFC ($t(18) = 9.63$ for average across the sub-regions within mPFC, $P < 0.001$) for both time periods with a significant increase during the targeting period (Fig. 5c & Fig. S6, top panel; $F(1,72) = 4.51$, $P = 0.03$), regardless of the seeds (MTL or mPFC; $F(1,72) = 0.00$, $P=0.98$). These results suggest that the default-mode network contributes more to the retrieval of the target location than the self-location to an external reference during the facing period. In contrast, the frontoparietal control network showed significantly negative connectivity with the MTL ($t(18) = -10.50$, $P < 0.001$) and mPFC ($t(18) = -6.55$, $P < 0.001$) during both task periods, indicating that the frontoparietal control network works competitively with MTL and mPFC areas of the default-mode network. This competitive effect was stronger during the targeting period (Fig. 5c $F(1,72) = 5.58$, $P = 0.02$, also see Fig. S6, middle panel;). Interestingly, despite both the MTL and mPFC being part of the default-mode network, they showed opposite connectivity patterns to the dorsal attention network during both periods (Fig. 5c & Fig. S6, bottom panel; $F(1,72) = 55.07$, $P < 0.001$); the MTL positively with the network while the mPFC negatively correlated with it. The connectivity between the MTL and the dorsal attention network increased from the facing to targeting period ($F(1,72) = 8.43$, $P = 0.005$). These results

suggested that the dorsal attention network, which contains the superior parietal lobule (SPL) that represented egocentric target location (Fig. 4a), showed increased coupling with the MTL during the targeting period. On the other hand, the mPFC only attenuated its amplitude of anti-correlated connectivity with the dorsal attention network, which may suggest that egocentric target location represented in the mPFC was not directly transmitted to the dorsal attention network. Considering the increased coupling between the mPFC and default-mode network including MTL areas during the targeting period (Fig. 5b&c), we hypothesize that the egocentric target location might be transferred from the mPFC to the SPL via the MTL.

Discussion

In this study, we examined neural representations of space defined by three objects and found that both the HPC and mPFC represented the object-based space around the participants. Interestingly, the HPC represented the object-based map when the participants locate their self-body in the environment constructed by the three objects, while the mPFC represented the map when the participants remembered the location of a target object relative to the self-body. These results suggest that the cognitive maps in different brain regions play different functional roles. In addition, during the targeting period, we found differential spatial representations across the MTL and mPFC: the MTL generally reinstated allocentric self-location, while the mPFC represented egocentric target location relative to self-location. Increased functional connectivity was observed between the MTL and mPFC under the necessity of the retrieval of the target location from the stored memory (targeting period) compared to when they actually faced the reference object to locate their self-body (facing period). These results suggest that mental representations of the external world formed by the coherent space and its constituent elements may be shared in the default-mode network including the MTL and mPFC. The special role of the mPFC in this scheme might be to select the object location based on the mnemonic information including the cognitive map and current self-location on it, which might be propagated from the MTL.

To examine the representation of spatial "*maps*" (Fig. 1b), the present task was designed to cancel out effects of a particular encoding experience related with the walking direction as well as a particular object identity that the participants viewed during the facing and targeting periods in each trial by balancing number of trials with each of those confounding factors in each map (see Methods). Therefore, the neural representation of the map information revealed by the RSA could not be explained by perceptual information in the present study. Moreover, the participants always stood on the center of the virtual

environment during the facing and targeting periods, during which the map effect was examined. Because of this task design, the map information does not directly indicate self-location information like place fields of place cells in the HPC (O'Keefe and Dostrovsky, 1971). On the other hand, the representations of place-fields are reportedly influenced by the animal's cognitive map, and the existence of cognitive maps could be most clearly demonstrated by a phenomenon known as "remapping", which reportedly occurs in populations of place cells in the rodent HPC (Moser et al., 2017). Therefore, it might be reasonable to interpret the map representations in the left mHPC during the facing period as experimental evidence of "remapping" of place cells in the human HPC even though the participants stood in the same position. However, holding this interpretation predicts that human place cells are localized in the left mHPC. This prediction is against consistent evidence from previous human studies reporting that the right HPC was more involved in encoding and retrieving spatial information than the left HPC (Abrahams et al., 1997; Maguire et al., 1997; Ekstrom et al., 2003; Doeller et al., 2008; Schinazi, 2013). The other possible interpretation for the map representation in the left mHPC is that it may encode an allocentric spatial relationship of the three objects itself. This interpretation is consistent with previous human imaging studies reporting contributions of the left HPC to the imagination of visual scenes, which could be constructed from multiple spatial elements (Addis et al., 2007; Bird et al., 2010). The specific role of the left HPC in relational memory was also reported in non-spatial information domains, including associative learning (Kumaran et al., 2009; Suarez-Jimenez et al., 2018) and social interactions (Tavares et al., 2015;). Taken together, it might be more reasonable to interpret that the clusters in the left mHPC was related to a coherent space constructed by the multiple objects rather than its influence on representations of individual spatial elements such as self-location or head direction. RSA also suggested the involvement of the PRC and PHC in MTL signaling the object identity and egocentric view

of their spatial layout, respectively, which might be used for constructing the coherent map from its constituents in the left mHPC. Future studies should address how the coherent map can be constructed by multiple objects in the MTL.

In contrast to the facing period, the representation of the map information was found in the mPFC but not in the HPC during the targeting period. In addition, the mPFC signaled the egocentric location of a targeting object, while the MTL concurrently signaled the allocentric self-location. Involvement of the mPFC in constructing goal-directed information in the current context is consistent with accumulating evidence showing that the mPFC contributes to decision making or action selection (Saxena et al., 1998; Gallagher et al., 1999; Feierstein, 2006; Spiers and Maguire, 2007; Kable and Glimcher, 2009; Young and Shapiro, 2011; Balaguer et al., 2016; Yamada et al., 2018). These previous studies consistently supported the notion that the mPFC function becomes obvious when an appropriate selection requires mnemonic information in addition to incoming perceptual information (Bradfield, 2015). In this study, together with perceptual information responsible for target object identity, mnemonic information such as the map information and allocentric self-location was required to solve the task. Considering that the MTL could provide all the necessary mnemonic information, a reasonable interpretation is that the mPFC was involved in the selection of a target location among alternatives rather than the recollection or generation of it.

In addition to the HPC and mPFC, the map information has been observed in other brain areas such as the angular gyrus (Seghier, 2013; Price et al., 2016), lateral temporal gyrus (Karnath, 2001; Himmelbach et al., 2006), and precuneus (Cavanna and Trimble, 2006) that also belong to the default-mode network. The brain areas in the default-mode network, particularly the MTL sub-regions except for the PRC represented allocentric self-location

during the targeting period. On the other hand, RSA analysis showed that widely-distributed brain regions were involved in the representation of the egocentric target object location not only in the default-mode network but also in the dorsal attention network and frontoparietal control network. The positive and negative functional connectivity between the dorsal attention network and the MTL and mPFC suggest that the egocentric target location signal is transmitted from the mPFC to the brain regions of the dorsal attention network, such as the SPL (Evans et al., 2016), via the MTL, which implies a pivotal functional role of MTL as a hub of mental representation of object signals.

Interestingly, the frontoparietal control network showed a strong negative correlation with both the MTL and mPFC during both the facing and targeting periods, although the lPFC in the frontoparietal control network represented both the map information and egocentric direction during the targeting period. In addition, the lPFC represented walking direction as well as character identity during both periods. These results suggest that the lPFC computes the target location independently of the default-mode network. The parallel contributions of the lPFC and MTL-mPFC in choosing the target location may reflect their different cognitive functions (Jimura et al., 2004). lPFC has long been considered as a center of executive functions (Funahashi, 2017; Miller et al., 2018) equipped with working memory (Andrews et al., 2011; Barbey et al., 2013; Brunoni and Vanderhasselt, 2014; Funahashi, 2017). In human fMRI studies, the lPFC has been shown to contribute to the retrieval of task-relevant information when more systematic thinking is required (Epstein et al., 2017; Javadi et al., 2017). In the present study, the behavioral task was designed to ensure participants neither actively maintained a spatial configuration of the human characters during the walking period nor any systematic strategy to solve the task, which was confirmed by the post-scanning test results. The greater signal for the cognitive map and the egocentric target location in the mPFC than that in the lPFC may reflect that the current spatial memory task

was enough easy to allow participants to depend only on the involuntary encoding and subsequent memory retrieval for their top-ceiling performance (Epstein et al., 2017; Javadi et al., 2017).

In contrast to previous memory/navigation studies, which examined brain functions using spatial environments consisting of immobile landmarks (e.g., stores) and/or landscapes (e.g., mountains) (Bird et al., 2010; Woollett and Maguire, 2011; Schinazi et al., 2013; Chadwick et al., 2015; Brown et al., 2016), the present study used a spatial environment constructed by only mobile objects that could become targets and references of self-location as well as determine the space (i.e., map) around oneself. This task design allowed us to extract a mental representation of the spatial environment consisting of the minimum essential constituents. This reductionist method could be useful for future studies investigating the construction and functional mechanisms of a cognitive map because of its simplicity. One critical concern might be whether the findings discovered by this reductionist method can be applied to a more complicated cognitive map consisting of large numbers of immobile spatial elements, which could be learned through extensive explorations over a long time period (e.g., the city of London) (Woollett and Maguire, 2011). Another related concern might be whether our brain system holds only one cognitive map or multiple ones at a time (Meister and Buffalo, 2018). For example, we may hold an object-based cognitive map consisting of relevant mobile objects such as same species, predators, and foods, while we may also hold the other cognitive map consisting of landmarks, landscapes and other immobile objects such as trees. Future studies should address the relationships of different types of cognitive maps (e.g., mobile vs immobile, short-term vs. long-term) and their underlying neural mechanisms.

The present study found neural representations of the space specified by objects around us. This object-based cognitive map seems to interact with representation of self-

location in HPC and to mediate a selection of egocentric target-location in mPFC, which would serve for leading us to the goal position. In addition to the spatial navigation, an existence of the object-based cognitive map may equip us with a space representation for persons separately from the background, which may serve for our social interactions (Damasio et al., 1994; Stolk et al., 2015) as well as the encoding and retrieval of episodic memory (Tulving, 2002; Squire and Wixted, 2011).

Supplemental Information

Supplemental Information includes six figures, two tables and two videos. The videos contain trial examples for Day 1 and Day 2. In the video of day 1, please note we only used examples of correct trials in which a green square of line was preented as feedback after the participant's response. File size: 21.5 MB; Video duration: 1.23 minute; File format: .mp4; Video codec: H.264; Aspect ratio: 1024 x 768.

Author Contributions

B.Z. and Y.N made the experimental design; B.Z. conducted all experiments and data analysis under supervision of Y.N.; B.Z. and Y.N. wrote the paper.

Acknowledgments

The present study was funded by National Natural Science Foundation of China Grant 31421003 (to Y.N.). Computational work was supported by resources provided by the High-performance Computing Platform of Peking University. We thank Li Sheng and Sun Pei for

453 helpful discussions, we also thank Arielle Tambini, Lusha Zhu, Koji Jimura, Rei Akaishi and

454 Cen Yang for comments on an early version of the manuscript.

Main figures

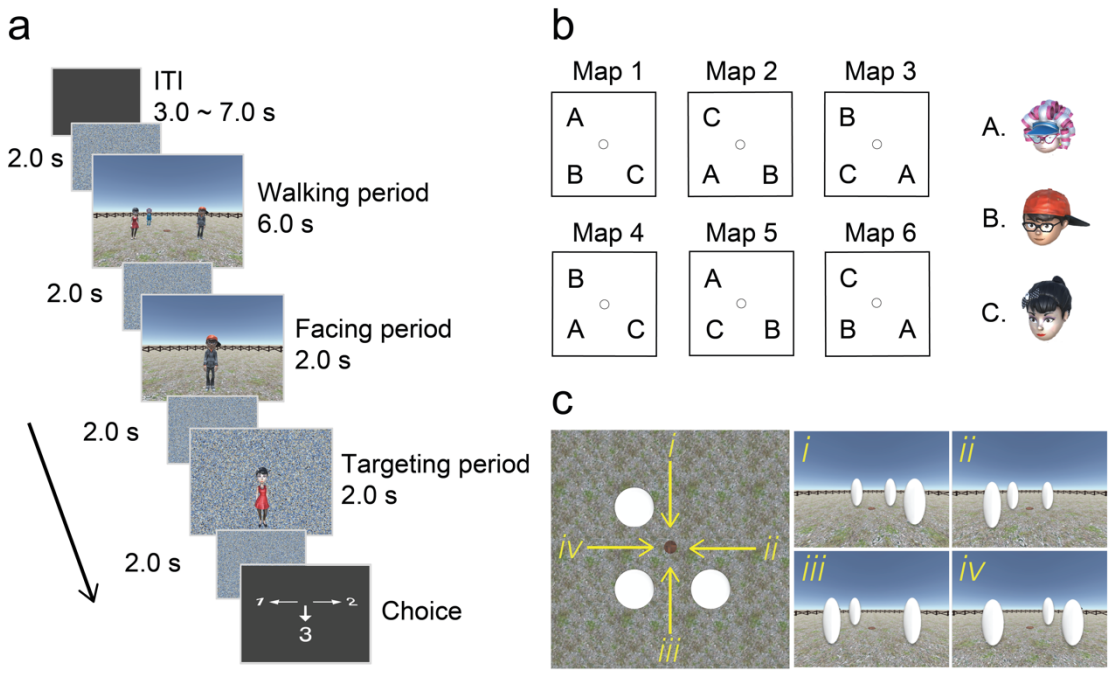

Figure 1: Task design. (a) spatial-memory task. Each trial consisted of three periods. In the walking period, participants walked toward three human characters using the first-person perspective and stopped on a wood plate. In the facing period, one of the human characters was presented, indicating the participant's current self-orientation. In the targeting period, a photo of another character was presented on the scrambled background. The participants chose the direction of the target character relative to their body upon presentation of a response cue. (b) Maps were defined by the relative position of the three human characters, while the unfilled dot represents the wood plate. (c) The walking directions were defined by the spatial layout of the three human characters from the participant's first-person perspective.

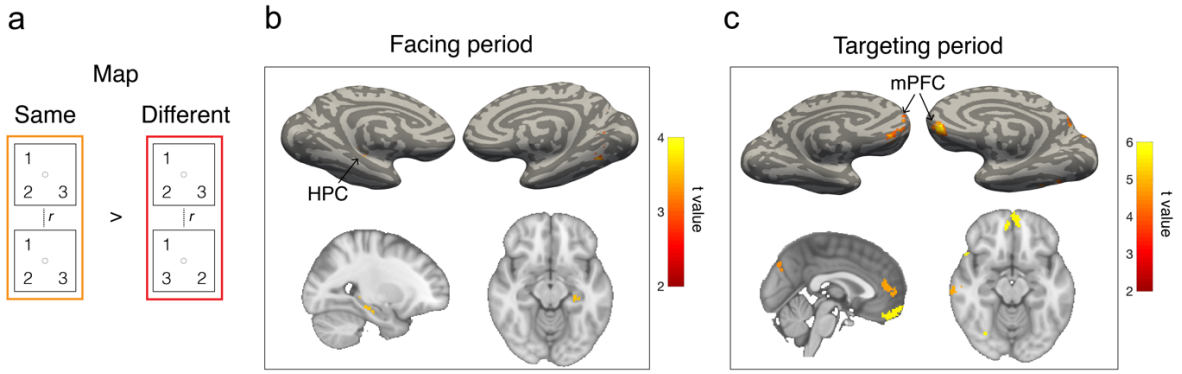

Figure 2: Neural representation of the map information in MTL and mPFC. (a) Schematic representation of decoding the cognitive map using RSA. (b) In the facing period, RSA revealed a cluster in the left middle HPC (mHPC; MNI coordinates: -28,-27,-16; shown on sagittal and transverse section) within the MTL ($P < 0.01$, initial threshold; $P < 0.05$, cluster-corrected for multiple comparison). (c) In the targeting period, clusters were revealed in the mPFC but not in the MTL ($P < 0.001$, initial threshold; $P < 0.05$, cluster-corrected for multiple comparison). A peak was revealed in the rectus within the mPFC (t value: 5.62; MNI coordinates: 4, 50, -18).

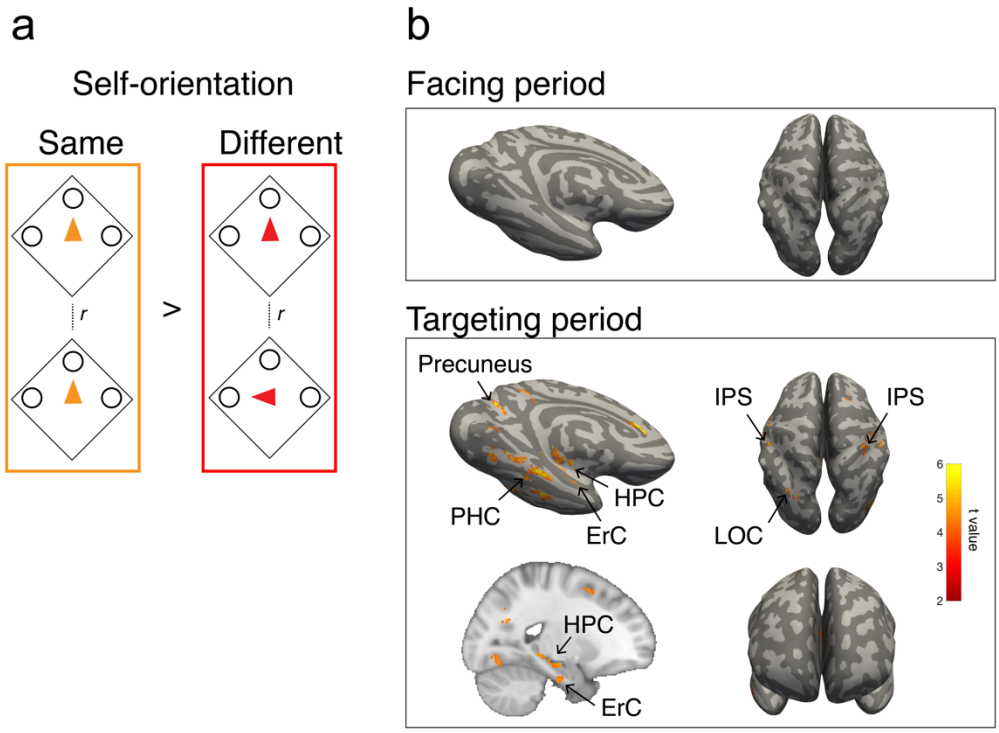

Figure 3: Neural representation of self-orientation on cognitive map. (a) Schematic representation of decoding participants' self-orientation. (b) In the facing period, no cluster was revealed even with the use of a more liberal threshold ($P < 0.01$, initial threshold; $P < 0.05$, cluster-corrected for multiple comparison). In the targeting period, clusters were revealed in the MTL (bilateral HPC, PHC, and left ErC) and self-motion areas (inferior parietal cortex, RSC, and lateral occipital cortex).

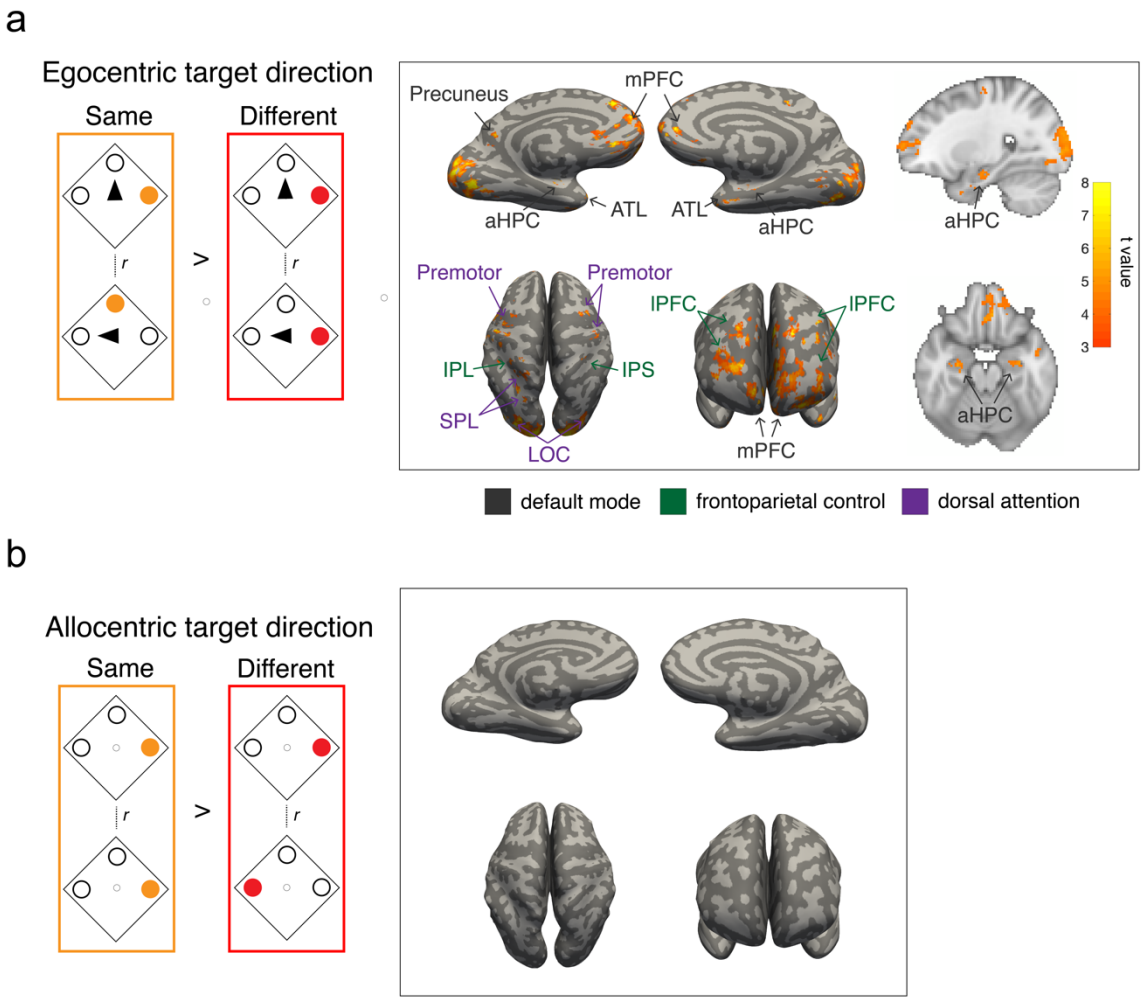

484

485 Figure 4: Neural representation of retrieved egocentric target location. (a) Left panel:
486 Schematic representation of decoding the egocentric direction of a target character. Right
487 panel: Clusters were revealed across a wide range of brain areas ($P < 0.001$, initial threshold;
488 $P < 0.05$, cluster-corrected for multiple comparison). Many of the clusters belonged to one of
489 the following three functional networks: the default-mode network, frontoparietal control
490 network, and dorsal attention network. The aHPC is shown on sagittal and transverse section
491 of volumn image for display purpose ($P < 0.001$, initial threshold; $P < 0.05$, cluster-corrected
492 for multiple comparison). (b) Left panel: Schematic representation of decoding allocentric
493 direction of a target character . Right panel: No clusters were revealed even with the use of a
494 liberal threshold ($P < 0.01$, initial threshold; $P < 0.05$, cluster-corrected for multiple
495 comparison).

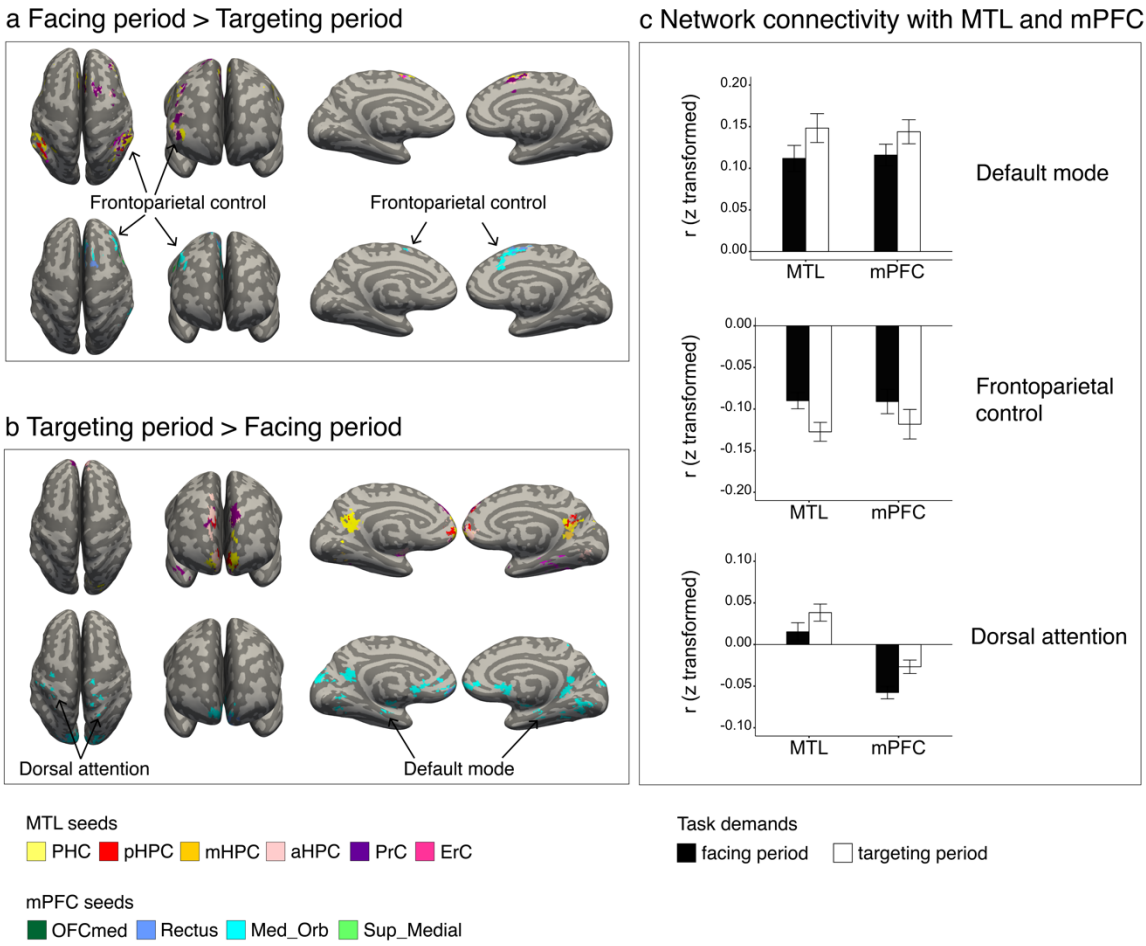

Figure 5: Increased default-mode network connectivity while locating a target compared with locating oneself. (a) The frontoparietal control network showed enhanced connectivity strength with the MTL and mPFC in the facing period compared to the targeting period ($P < 0.001$, initial threshold; $P < 0.05$, cluster-corrected for multiple comparison). (b) The default-mode network and dorsal attention network showed enhanced connectivity strength with the MTL and mPFC in the targeting period compared to the facing period ($P < 0.001$, initial threshold; $P < 0.05$, cluster-corrected for multiple comparison). (c) The mean connectivity strength of MTL and mPFC sub-regions with three networks, respectively. Note that the connectivity between default-mode network and MTL/mPFC was examined using default-mode network mask without the MTL/mPFC, respectively.

Methods

Participants

Nineteen right-handed university students with normal or corrected-to-normal vision were recruited from Peking University (12 females, 7 males). The average age of the participants was 24.9 years (range: 18–30 years). All participants had no history of psychiatric or neurological disorders and gave their written informed consent prior to the start of the experiment, which was approved by the Research Ethics Committee of Peking University.

Task design

Virtual environment. We programmed a 3D virtual environment using Unity software (Unity Technologies, San Francisco). The environment was designed with a circular fence as a boundary (48 virtual meters in diameter), a flat grassy ground, a uniform blue sky, and with a wood plate surrounded by four vertices of a square placed in the center (Fig. 1b, 4.7 virtual meters for side length). Three human characters (Mixamo, San Francisco, https://www.mixamo.com) were placed on three of the vertices in each trial. A map was defined by the relative relationship of the three human characters (Fig. 1b). From the six possible maps, three of them were pseudo-randomly selected for each participant to collect enough number of trials' data for each condition during the allowable range of scanning duration. The maps were the only environmental cues relevant to the task requirement, no distal cues were used outside the boundary. Participants performed the task using the first-person perspective with a 90° field of view (aspect ratio = 4:3), they had never seen a top-down view of the virtual environment.

Walking period. Participants walked from one of four starting locations near the circular boundary (4 virtual meters from the boundary) toward the human characters (Fig. 1c) and

stopped on the wood plate. The visual stimuli (spatial environment viewed from first-person perspective) were determined by the combination of the map and walking direction, in other words, each map was presented by four different visual stimuli that were determined by the starting position (Fig. 1c). Importantly, participants were blinded to the map concept throughout the task. The walking period lasted for 6.0 s, during which each character had a 20.6% probability of nodding its head at a random time point between the start and end of walking. There was a 50%, 38.9%, 10.2%, and 0.9% probability for 0, 1, 2, and 3 characters to nod head in each trial; we subjectively selected a 20.6% head-nodding probability for each character to ensure an approximately equal number of trials with head-nodding and no head-nodding. During the walking period, participants were required to pay attention to the heads of the human characters rather than to memorize their spatial arrangement. The height of the participants was 1.8 virtual meters from the ground, which was the same as that of the human characters. No response was required during the walking period.

Two tasks were completed in two consecutive days. On day 1, the participants performed an HND task that did not include spatial-memory trials. On day 2, participants performed a spatial-memory task.

Head-nodding detection (HND) task. Participants performed 144 randomly ordered HND trials in a behavioral experimental room. In each trial, a photo of one of the characters was presented on a screen after the walking period, and participants were asked to indicate whether the character nodded its head or not (Fig. S1a). For this task, there was a 50% chance that the character in the presented photo nodded its head. Feedback was given after the participants had responded with either green (correct) or red (incorrect) photo border. The stimuli were rendered on a PC and presented on a 27-inch LCD monitor (ViewSonic XG2730) with a screen resolution of 1024 x 768. The HND task was used to examine whether participants paid attention to head-nodding rather than memorizing the spatial

arrangement of the characters, which would be indicated by high success rates in the head-nodding test.

Spatial-memory task. During this task, participants performed 144 spatial-memory trials (90%) and 16 HND trials (10%) that lasted ~ 70 min in an MRI scanner. Participants were notified that the remuneration depended only on the performance in the HND trials although they were also encouraged to perform the spatial memory task as best as they could (videos of trial examples are available online for both tasks). The trial-type (i.e., HND or memory task) was distinguishable after the walking period by subsequent stimuli. In the spatial-memory task, participants experienced a "facing period" and a "targeting period" sequentially after the walking period. In the facing period, their self-orientation was changed immediately to one of the human characters (facing-character) without viewpoint transition, and a character with the environment background was presented for 2.0 s with the other two characters being invisible, the participants were instructed to face the character. In the targeting period, a photo of another character (targeting-character) was presented as a target on a scrabbled background for 2.0 s. Each of the three experimental periods was followed by a 2.0-s delay (noise screen). At the end of each trial, participants indicated the direction of the target character relative to their self-body by pressing a button when a cue presented on the screen; no feedback was shown for both trial-types (Fig. 1a). The spatial-memory task contained four experimental sessions, each containing a spatial information combination of 3 maps x 4 walking directions x 3 facing-character identities in each session, with targeting-characters balanced across sessions. After scanning, all participants completed a post-scanning interview and reported the strategy they used to perform the task (Table. S2).

fMRI data acquisition

Imaging data were collected using a 3T Siemens Prisma scanner equipped with a 20-channel receiver head coil. Functional data were acquired with a Multi-band Echo Planer imaging (EPI) sequence (TR = 2000 ms, TE = 30 ms, matrix size: 112 × 112 x 62, flip angle: 90°, gap = 0 mm; resolution: 2 × 2 × 2.3 mm^3, number of slices: 62, slice thickness: 2 mm, slice orientation: transversal), four experimental sessions were collected with, on average, 478, 476, 473, 475 TRs, respectively. A high-resolution T1-weighted three-dimensional anatomical data set was collected to aid in registration (MPRAGE, TR = 2530 ms, TE = 2.98 ms, matrix size: 448 x 512 x 192, flip angle: 7°, resolution: 0.5 × 0.5 × 1 mm^3 , number of slices: 192, slice thickness: 1 mm, slice orientation: sagittal). During scanning, experimental stimuli were presented through a Sinorad LCD projector (Shenzhen Sinorad Medical Electronics) onto a 33-inch rear-projection screen located over the subject's head with a resolution of 1024 x 768 and viewed with an angled mirror positioning on the head coil.

fMRI preprocessing

Functional data for each session were preprocessed independently using FSL FEAT (FMRIB's Software Library, version 6.00, https://fsl.fmrib.ox.ac.uk/fsl/fslwiki; Woolrich et al., 2001; Woolrich et al., 2004). For each session, the first three functional volumes were discarded to allow for T1 equilibration, and the remaining functional volumes were slice-time corrected, realigned to the first image, and high-pass filtered at 100 s. For group-level statistics, each session's functional data were registered to a T1-weighted standard image (MNI152) using FSL FLIRT (Jenkinson and Smith, 2001), and this procedure also resampled the functional voxels into a 2 x 2 x 2 mm resolution. For RSA, data were left unsmoothed to preserve any fine-grained spatial information (Chadwick et al., 2012). For functional connectivity analysis, data were smoothed using a 5 mm FWHM Gaussian kernel and were high-pass filtered at 0.01 Hz to remove low-frequency signal drifts.

607

608 **Anatomical masks**

609 We manually delineated the MTL, including the HPC, PHC, PRC, and ERC on each
610 participant's native space using established protocols (Insausti et al., 1998; Pruessner et al.,
611 2000; Pruessner et al., 2002; Duvernoy, 2005), as well as a delineating software ITK-SNAP
612 (www.itksnap.org). The HPC was further divided into its anterior, middle, and posterior parts
613 given the anatomical and functional variability along the HPC long axis (Poppenk et al.,
614 2013), the anterior border of pHPC and the posterior border of aHPC were defined by the
615 appearance of the crus of the fornix and the uncal apex relative to mHPC along the coronal
616 orientation, respectively (Pruessner et al., 2000; Poppenk et al., 2013). For PFC sub-regions,
617 we used the AAL template (Rolls et al., 2015), and selected four mPFC sub-regions for ROI-
618 analysis, which included the rectus, medial orbital gyrus (OFCmed), medial orbital frontal
619 gyrus (Med_Orb), and superior medial frontal gyrus (Sup_Med). All ROIs were resampled
620 and aligned with the functional volumes, and voxels outside of the brain were excluded.

621

622 **Representational similarity analysis (RSA)**

623 Task-relevant information was decoded using RSA. We tried to dissociate the neural effect of
624 facing and targeting period based on 4 s duration from each period onset to the end of
625 following noise period (Zeithamova et al., 2017). First, the trial-based multi-voxel activity
626 patterns of two periods were obtained by creating two separate univariate general linear
627 models (GLM). In each GLM, the 4 s blood-oxygen-level-dependent (BOLD) signals of 36
628 trials (a session) were modeled using boxcar regressors. In addition to the 36 trial-based
629 regressors of interest, nuisance regressors were included, which included twelve regressors
630 for modeling the visual patterns of the walking period determined by the maps and walking
631 directions, three for modeling the character identities in the remaining period (for example, in

632 the facing period GLM, three targeting characters were specified as nuisance regressors
633 rather than the facing characters), four for modeling head-nodding detection trials, three for
634 modeling 3 directional cues in the response period, and six motion parameters. This
635 procedure generated 36 trial-based multi-voxel patterns in participant's native space (2 x 2 x
636 2.3 mm voxels) for each period, those multi-voxel patterns were normalized prior to
637 subsequent analysis by subtracting the grand mean pattern of the 36 multi-voxel patterns for
638 each session (Vass and Epstein, 2013).
639 Searchlight-based RSA. Next, we computed the representational similarity for each spatial
640 information based on the multi-voxel patterns using a searchlight-based RSA (Libby et al.,
641 2014; Chadwick et al., 2015), which was conducted using custom Matlab (version R2018b,
642 www.mathworks.com/matlab/) scripts. In detail, a sphere with a 6 mm radius was constructed
643 (85 voxels per sphere) for each brain voxel, and the spheres near the edge of the brain with
644 fewer than ten voxels were excluded from the analysis. The activity parameters within each
645 sphere were extracted from each of the 36 multi-voxel patterns, resulting in a 36-column by
646 n-row (number of voxels within the sphere) matrix. The pattern similarity was then calculated
647 between each column-by-column pair using Pearson's correlation, and was normalized using
648 Fisher's r-to-z transformation. This procedure finally generated a 36-by-36 correlation matrix
649 for each period in each brain voxel. Next, given that a multi-voxel pattern contains the
650 combination of multiple spatial information, we conducted a GLM for each correlation
651 matrix by specifying multiple categorical regressors to rule out potential influences. Each
652 spatial representation represented specific spatial information and used either indicator "1
653 (same)" or " 0 (different)" that corresponded with the correlation coefficient of a given
654 column-to-row cell of the correlation matrix. For the facing period, the GLM contained five
655 categorical regressors, which included the (1) "map", (2) "walking direction", and (3)
656 "facing-character identity". Since the participants reported thinking about their bodies

657 rotating between the walking direction and self-orientation relative to the environment, we
658 also added the (4) "rotation angle" (turn left/right 45°, turn left/right 135°), and (5) their
659 "self-orientation" into the GLM. For the targeting period, seven regressors were built, which
660 included: (1) "map", (2) "walking direction", (3-4) participants' "rotation angle" and "self-
661 orientation", (5) "targeting-character identity", and (6-7) "egocentric and allocentric position
662 of target-character". It is important to note that the "facing-character identity" was not
663 included in the targeting period GLM since the effect of each facing character was regressed
664 out in the GLM computing of multi-voxel activity patterns. r^2 was computed and ranged from
665 0 to 0.03 for the facing period GLM, and 0 to 0.04 for the targeting period GLM (Table S1).
666 Each regressor's parameter was then assigned to the center voxel of each sphere so that a
667 whole-brain statistical parametric mapping could be generated for each spatial information
668 for each period, with those spatial representations being finally averaged across the four
669 scanner sessions. By using this method, spatial information should be successfully decoded if
670 the regressors stably predict the correlation coefficients in any voxels.
671
672 *ROI-based RSA*. To validate the spatial representations, we further conducted an
673 independent RSA using anatomical ROIs of MTL and PFC sub-regions. We reasoned that
674 since searchlight analysis identifies the spatial representations as clusters in small portions of
675 anatomical regions, if those representations are stable enough, the corresponding anatomical
676 regions, on average, should show a clear increasing tendency in similarity when spatial
677 information between trial-pairs are similar compared to different such that they match the
678 searchlight results. To test this, we separated each ROI into the left and right hemispheres and
679 generated 20 anatomical masks (Fig. S4a; 12 for the MTL and 8 for the mPFC). The mPFC
680 masks were normalized into the participants' native space. The RSA procedure for each ROI
681 was similar to searchlight analysis, which produced a 36-by-36 correlation matrix for each

period. Next, for each spatial information (e.g., map), the correlation matrix elements were z-transformed and were grouped into "same" and "different" conditions. The mean values of the matrix elements in the same condition was subtracted by those in the different condition in each session (36 trials). The subtracted values were averaged across the four sessions for each participant. We referred to this averaged value as a discrimination score. We tested whether or not the discrimination score was positive among the participants using one-sample t-test (one-tail).

Functional connectivity (FC) analysis

To investigate the functional networks for different task demands, we examined the whole-brain FC using each sub-region of MTL and mPFC as seed (Fig. S4a; 12 for the MTL and 8 for the mPFC). In detail, we first removed the nuisance covariates from the preprocessed functional data by creating a GLM, which specified the signal averaged over the lateral ventricles, white matter, and whole brain, six motion parameters, and their derivatives as regressors. The residual signal was bandpass-filtered, leaving signals within the frequency range 0.01 to 0.1 Hz, and was shifted by two TR intervals (4 s) for subsequent analysis (Tompary and Davachi, 2017). We computed a regional time course for each anatomical mask in each of facing and targeting period. To do this, we averaged signals over the mask at each TR within the period, and then concatenated the two values in one trial with those in the next trial within a session (Ranganath et al., 2005). The regional time course for each anatomical mask was correlated with the time course of each voxel in the rest of the brain, resulting in a whole-brain correlation map for each period in each scanning session. The correlation maps were averaged across four scanning sessions for each participant, and were then submitted to a two-tailed t-test for group level statistics.

Each cluster, which derived from the contrast analysis in connectivity between facing and targeting period based on an initial threshold of $p=0.001$, was assigned to each of the

three networks based on previous literatures: default-mode network, frontoparietal control network, and dorsal attention network (Vincent et al., 2008; Schacter et al., 2012; Gelström and Graziano., 2017). In the present study, default-mode network contains the clusters of mPFC, MTL, posterior cingulate cortex, and anterior temporal gyrus; frontoparietal control network contains the clusters of paracingulate gyrus, lateral PFC, and inferior parietal lobule; dorsal attention network contains the clusters of occipital pole, lateral occipital cortex, cuneal cortex, lingual gyrus, superior parietal lobule, and postcentral gyrus (Fig. S4b). To examine modulation effects on the connectivity of MTL/mPFC with the large-scale networks by different task demands, we computed mean connectivity between each of MTL and mPFC subregions with each network. For the default-mode network, we prepared for two masks, in which the MTL or mPFC was removed for the examinations of its connectivity with the default-mode network.

Statistics

For searchlight-based RSA, we used an initial threshold of $p < 0.001$. If no clusters were revealed, a more liberal threshold of $p < 0.01$ was used. For whole brain FC analysis, an initial threshold of $p<0.001$ was used to identify robust network patterns. For both searchlight-based RSA and whole brain FC analysis, the reliability of significant effects was tested using a non-parametric statistical inference that does not make assumptions about the distribution of the data, the test was conducted with the FSL randomise package (version v2.9, http://fsl.fmrib.ox.ac.uk/fsl/fslwiki/Randomise) (Nichols and Holmes, 2002; Winkler et al., 2014) using 5000 random sign-flips and threshold-free clustering. We then reported voxels that were significant at $p < 0.05$ after correcting for multiple comparisons across the entire brain. ROI-based RSA used one-tailed one sample t-test to examine the significance of each anatomical mask. Paired t-test was used to examine the difference in connectivity

732 among MTL and mPFC subregions between task demands. All t-test results were Bonferroni-
733 corrected for multiple comparison (alpha < 0.05). Analysis of variance (ANOVA) was used
734 to test the influence in connectivity between MTL/mPFC and large-scale functional network
735 along time periods.
736

737 **Reference**

738

739 Abrahams, S., Pickering, A., Polkey, C. E., & Morris, R. G. (1997). Spatial memory deficits
740 in patients with unilateral damage to the right hippocampal
741 formation. Neuropsychologia, 35(1), 11-24.
742
743 Andrews, S. C., Hoy, K. E., Enticott, P. G., Daskalakis, Z. J., & Fitzgerald, P. B. (2011).
744 Improving working memory: the effect of combining cognitive activity and anodal
745 transcranial direct current stimulation to the left dorsolateral prefrontal cortex. Brain
746 stimulation, 4(2), 84-89.
747
748 Addis, D. R., Wong, A. T., & Schacter, D. L. (2007). Remembering the past and imagining
749 the future: common and distinct neural substrates during event construction and
750 elaboration. Neuropsychologia, 45(7), 1363-1377.
751
752 Barbey, A. K., Koenigs, M., & Grafman, J. (2013). Dorsolateral prefrontal contributions to
753 human working memory. cortex, 49(5), 1195-1205.
754
755 Brunoni, A. R., & Vanderhasselt, M. A. (2014). Working memory improvement with non-
756 invasive brain stimulation of the dorsolateral prefrontal cortex: a systematic review and meta-
757 analysis. Brain and cognition, 86, 1-9.
758
759 Bird, C. M., Capponi, C., King, J. A., Doeller, C. F., & Burgess, N. (2010). Establishing the
760 boundaries: the hippocampal contribution to imagining scenes. Journal of
761 Neuroscience, 30(35), 11688-11695.
762
763 Buffalo, E.A. (2015). Bridging the gap between spatial and mnemonic views of the
764 hippocampal formation. Hippocampus *25*, 713-718.
765
766 Balaguer, J., Spiers, H., Hassabis, D., & Summerfield, C. (2016). Neural mechanisms of
767 hierarchical planning in a virtual subway network. Neuron, 90(4), 893-903.
768
769 Bradfield, L. A., Dezfouli, A., van Holstein, M., Chieng, B., & Balleine, B. W. (2015).
770 Medial orbitofrontal cortex mediates outcome retrieval in partially observable task
771 situations. Neuron, 88(6), 1268-1280.
772
773 Brown, T. I., Carr, V. A., LaRocque, K. F., Favila, S. E., Gordon, A. M., Bowles, B., ... &
774 Wagner, A. D. (2016). Prospective representation of navigational goals in the human
775 hippocampus. Science, 352(6291), 1323-1326.
776
777 Cavanna, A.E., and Trimble, M.R. (2006). The precuneus: a review of its functional anatomy
778 and behavioural correlates. Brain : a journal of neurology 129, 564-583.
779
780 Campbell, K.L., Madore, K.P., Benoit, R.G., Thakral, P.P., and Schacter, D.L. (2018).
781 Increased hippocampus to ventromedial prefrontal connectivity during the construction of
782 episodic future events. Hippocampus 28, 76-80.
783
784 Chadwick, M. J., Jolly, A. E., Amos, D. P., Hassabis, D., & Spiers, H. J. (2015). A goal
785 direction signal in the human entorhinal/subicular region. Current Biology, 25(1), 87-92.

Chadwick, M. J., Bonnici, H. M., & Maguire, E. A. (2012). Decoding information in the human hippocampus: a user's guide. Neuropsychologia, 50(13), 3107-3121.

Duvernoy, H. M. (2005). The human hippocampus: functional anatomy, vascularization and serial sections with MRI. Springer Science & Business Media.

Damasio, H., Grabowski, T., Frank, R., Galaburda, A.M., and Damasio, A.R. (1994). The return of Phineas Gage: clues about the brain from the skull of a famous patient. Science 264, 1102-1105.

Doeller, C. F., King, J. A., & Burgess, N. (2008). Parallel striatal and hippocampal systems for landmarks and boundaries in spatial memory. Proceedings of the National Academy of Sciences, 105(15), 5915-5920.

Ekstrom, A.D., Kahana, M.J., Caplan, J.B., Fields, T.A., Isham, E.A., Newman, E.L., and Fried, I. (2003). Cellular networks underlying human spatial navigation. Nature *425*, 184-188.

Eichenbaum, H. (2017). The role of the hippocampus in navigation is memory. Journal of neurophysiology 117, 1785-1796.

Epstein, R.A., Patai, E.Z., Julian, J.B., and Spiers, H.J. (2017). The cognitive map in humans: spatial navigation and beyond. Nature neuroscience 20, 1504-1513.

Evans, T., Bicanski, A., Bush, D., & Burgess, N. (2016). How environment and self-motion combine in neural representations of space. The Journal of physiology, 594(22), 6535-6546.

Feierstein, C. E., Quirk, M. C., Uchida, N., Sosulski, D. L., & Mainen, Z. F. (2006). Representation of spatial goals in rat orbitofrontal cortex. Neuron, 51(4), 495-507.

Funahashi, S. (2017). Prefrontal Contribution to Decision-Making under Free-Choice Conditions. Frontiers in neuroscience 11, 431.

Gaesser, B., Spreng, R. N., McLelland, V. C., Addis, D. R., & Schacter, D. L. (2013). Imagining the future: evidence for a hippocampal contribution to constructive processing. Hippocampus, 23(12), 1150-1161.

Gallagher, M., McMahan, R. W., & Schoenbaum, G. (1999). Orbitofrontal cortex and representation of incentive value in associative learning. Journal of Neuroscience, 19(15), 6610-6614.

Gelström, K. M., & Graziano, M. S. (2017). The inferior parietal lobule and temporoparietal junction: a network perspective. Neuropsychologia, 105, 70-83.

Himmelbach, M., Erb, M., and Karnath, H.O. (2006). Exploring the visual world: the neural substrate of spatial orienting. NeuroImage 32, 1747-1759.

Hargreaves, E.L., Rao, G., Lee, I., and Knierim, J.J. (2005). Major dissociation between medial and lateral entorhinal input to dorsal hippocampus. Science 308, 1792-1794.

836 Hassabis, D., & Maguire, E. A. (2007). Deconstructing episodic memory with
837 construction. Trends in cognitive sciences, 11(7), 299-306.
838
839 Insausti, R., Juottonen, K., Soininen, H., Insausti, A. M., Partanen, K., Vainio, P., ... &
840 Pitkänen, A. (1998). MR volumetric analysis of the human entorhinal, perirhinal, and
841 temporopolar cortices. American Journal of Neuroradiology, 19(4), 659-671.
842

843 Javadi, A.H., Emo, B., Howard, L.R., Zisch, F.E., Yu, Y., Knight, R., Pinelo Silva, J., and
844 Spiers, H.J. (2017). Hippocampal and prefrontal processing of network topology to simulate
845 the future. Nature communications 8, 14652.
846
847 Jenkinson, M., & Smith, S. (2001). A global optimisation method for robust affine
848 registration of brain images. Medical image analysis, 5(2), 143-156.
849
850 Jimura, K., Konishi, S., and Miyashita, Y. (2004). Dissociable concurrent activity of lateral
851 and medial frontal lobe during negative feedback processing. NeuroImage *22*, 1578-1586.
852
853 Karnath, H. O. (2001). New insights into the functions of the superior temporal
854 cortex. Nature Reviews Neuroscience, 2(8), 568.
855
856 Kumaran, D., Summerfield, J. J., Hassabis, D., & Maguire, E. A. (2009). Tracking the
857 emergence of conceptual knowledge during human decision making. Neuron, 63(6), 889-901.
858
859 Kriegeskorte, N., Goebel, R., & Bandettini, P. (2006). Information-based functional brain
860 mapping. Proceedings of the National Academy of Sciences, 103(10), 3863-3868.
861
862 Kriegeskorte, N., Mur, M., Ruff, D. A., Kiani, R., Bodurka, J., Esteky, H., ... & Bandettini, P.
863 A. (2008). Matching categorical object representations in inferior temporal cortex of man and
864 monkey. Neuron, 60(6), 1126-1141.
865
866 Kable, J.W., and Glimcher, P.W. (2009). The neurobiology of decision: consensus and
867 controversy. Neuron *63*, 733-745.
868
869 Konishi, S., Wheeler, M.E., Donaldson, D.I., and Buckner, R.L. (2000). Neural correlates of
870 episodic retrieval success. NeuroImage *12*, 276-286.
871
872 Libby, L. A., Hannula, D. E., & Ranganath, C. (2014). Medial temporal lobe coding of item
873 and spatial information during relational binding in working memory. Journal of
874 Neuroscience, 34(43), 14233-14242.
875
876 Meister, M.L.R., and Buffalo, E.A. (2018). Neurons in primate entorhinal cortex represent
877 gaze position in multiple spatial reference frames. The Journal of neuroscience : the official
878 journal of the Society for Neuroscience.
879
880 Miller, E. K., Lundqvist, M., & Bastos, A. M. (2018). Working Memory 2.0. Neuron, 100(2),
881 463-475.
882
883 Moser, E.I., Moser, M.B., and McNaughton, B.L. (2017). Spatial representation in the
884 hippocampal formation: a history. Nature neuroscience 20, 1448-1464.

Maguire, E. A., Frackowiak, R. S., & Frith, C. D. (1997). Recalling routes around London: activation of the right hippocampus in taxi drivers. Journal of neuroscience, 17(18), 7103-7110.

McCormick, C., Ciaramelli, E., De Luca, F., and Maguire, E.A. (2018). Comparing and Contrasting the Cognitive Effects of Hippocampal and Ventromedial Prefrontal Cortex Damage: A Review of Human Lesion Studies. Neuroscience 374, 295-318.

Nakazawa, K., Quirk, M.C., Chitwood, R.A., Watanabe, M., Yeckel, M.F., Sun, L.D., Kato, A., Carr, C.A., Johnston, D., Wilson, M.A., et al. (2002). Requirement for hippocampal CA3 NMDA receptors in associative memory recall. Science 297, 211-218.

Nichols, T. E., & Holmes, A. P. (2002). Nonparametric permutation tests for functional neuroimaging: a primer with examples. Human brain mapping, 15(1), 1-25.

Naya, Y., and Suzuki, W.A. (2011). Integrating what and when across the primate medial temporal lobe. Science 333, 773-776.

Naya, Y., Yoshida, M., and Miyashita, Y. (2001). Backward spreading of memory-retrieval signal in the primate temporal cortex. Science *291*, 661-664.

O'Keefe, J., & Dostrovsky, J. (1971). The hippocampus as a spatial map: preliminary evidence from unit activity in the freely-moving rat. Brain research.

Pruessner, J. C., Li, L. M., Serles, W., Pruessner, M., Collins, D. L., Kabani, N., ... & Evans, A. C. (2000). Volumetry of hippocampus and amygdala with high-resolution MRI and three-dimensional analysis software: minimizing the discrepancies between laboratories. Cerebral cortex, 10(4), 433-442.

Pruessner, J. C., Köhler, S., Crane, J., Pruessner, M., Lord, C., Byrne, A., ... & Evans, A. C. (2002). Volumetry of temporopolar, perirhinal, entorhinal and parahippocampal cortex from high-resolution MR images: considering the variability of the collateral sulcus. Cerebral Cortex, 12(12), 1342-1353.

Packard, M.G., and McGaugh, J.L. (1996). Inactivation of hippocampus or caudate nucleus with lidocaine differentially affects expression of place and response learning. Neurobiology of learning and memory 65, 65-72.

Poppenk, J., Evensmoen, H. R., Moscovitch, M., & Nadel, L. (2013). Long-axis specialization of the human hippocampus. Trends in cognitive sciences, 17(5), 230-240.

Price, A. R., Peelle, J. E., Bonner, M. F., Grossman, M., & Hamilton, R. H. (2016). Causal evidence for a mechanism of semantic integration in the angular gyrus as revealed by high-definition transcranial direct current stimulation. Journal of Neuroscience, 36(13), 3829-3838.

Ranganath, C., Heller, A., Cohen, M. X., Brozinsky, C. J., & Rissman, J. (2005). Functional connectivity with the hippocampus during successful memory formation. Hippocampus, 15(8), 997-1005.

Ranganath, C., & Ritchey, M. (2012). Two cortical systems for memory-guided behaviour. Nature Reviews Neuroscience, 13(10), 713.

Rolls, E. T., Joliot, M., & Tzourio-Mazoyer, N. (2015). Implementation of a new parcellation of the orbitofrontal cortex in the automated anatomical labeling atlas. Neuroimage, 122, 1-5.

Redish, A.D., and Touretzky, D.S. (1998). The role of the hippocampus in solving the Morris water maze. Neural computation 10, 73-111.

Seghier, M. L. (2013). The angular gyrus: multiple functions and multiple subdivisions. The Neuroscientist, 19(1), 43-61.

Suarez-Jimenez, B., Bisby, J. A., Horner, A. J., King, J. A., Pine, D. S., & Burgess, N. (2018). Linked networks for learning and expressing location-specific threat. Proceedings of the National Academy of Sciences, 115(5), E1032-E1040.

Spiers, H. J., & Maguire, E. A. (2007). A navigational guidance system in the human brain. Hippocampus, 17(8), 618-626.

Schinazi, V. R., Nardi, D., Newcombe, N. S., Shipley, T. F., & Epstein, R. A. (2013). Hippocampal size predicts rapid learning of a cognitive map in humans. Hippocampus, 23(6), 515-528.

Squire, L.R., and Wixted, J.T. (2011). The cognitive neuroscience of human memory since H.M. Annual review of neuroscience 34, 259-288.

Schacter, D.L., Addis, D.R., and Buckner, R.L. (2007). Remembering the past to imagine the future: the prospective brain. Nature reviews Neuroscience 8, 657-661.

Spreng, R. N., & Schacter, D. L. (2011). Default network modulation and large-scale network interactivity in healthy young and old adults. Cerebral Cortex, 22(11), 2610-2621.

Schacter, D.L. (2012). Adaptive constructive processes and the future of memory. The American psychologist 67, 603-613.

Schacter, D. L., Addis, D. R., Hassabis, D., Martin, V. C., Spreng, R. N., & Szpunar, K. K. (2012). The future of memory: remembering, imagining, and the brain. Neuron, 76(4), 677-694.

Stolk, A., D'Imperio, D., di Pellegrino, G., and Toni, I. (2015). Altered communicative decisions following ventromedial prefrontal lesions. Current biology : CB 25, 1469-1474.

Saxena, S., Brody, A. L., Schwartz, J. M., & Baxter, L. R. (1998). Neuroimaging and frontal-subcortical circuitry in obsessive-compulsive disorder. The British Journal of Psychiatry, 173(S35), 26-37.

Suzuki, W., and Naya, Y. (2011). Two routes for remembering the past. Cell *147*, 493-495.

Suzuki, W.A., and Naya, Y. (2014). The perirhinal cortex. Annual review of neuroscience *37*, 39-53.

Tolman, E. C. (1948). Cognitive maps in rats and men. Psychological review, 55(4), 189.

Tavares, R. M., Mendelsohn, A., Grossman, Y., Williams, C. H., Shapiro, M., Trope, Y., & Schiller, D. (2015). A map for social navigation in the human brain. Neuron, 87(1), 231-243.

Tulving, E. (2002). Episodic memory: from mind to brain. Annual review of psychology, 53(1), 1-25.

Tompary, A., & Davachi, L. (2017). Consolidation promotes the emergence of representational overlap in the hippocampus and medial prefrontal cortex. Neuron, 96(1), 228-241.

Vincent, J. L., Kahn, I., Snyder, A. Z., Raichle, M. E., & Buckner, R. L. (2008). Evidence for a frontoparietal control system revealed by intrinsic functional connectivity. Journal of neurophysiology, 100(6), 3328-3342.

Vass LK, Epstein RA (2013) Abstract representations of location and facing direction in the human brain. J Neurosci 33:6133–6142. CrossRef Medline

Woollett, K., & Maguire, E. A. (2011). Acquiring "the Knowledge" of London's layout drives structural brain changes. Current biology, 21(24), 2109-2114.

Winkler, A. M., Ridgway, G. R., Webster, M. A., Smith, S. M., & Nichols, T. E. (2014). Permutation inference for the general linear model. Neuroimage, 92, 381-397.

Wang, C., Chen, X., Lee, H., Deshmukh, S.S., Yoganarasimha, D., Savelli, F., and Knierim, J.J. (2018). Egocentric coding of external items in the lateral entorhinal cortex. Science 362, 945-949.

Woolrich, M. W., Ripley, B. D., Brady, M., & Smith, S. M. (2001). Temporal Autocorrelation in Univariate Linear Modeling of FMRI Data. NeuroImage, 14(6), 1370–1386.

Woolrich, M. W., Behrens, T. E. J., & Smith, S. M. (2004). Constrained linear basis sets for HRF modelling using Variational Bayes. NeuroImage, 21(4), 1748–1761.

Wikenheiser, A. M., & Schoenbaum, G. (2016). Over the river, through the woods: cognitive maps in the hippocampus and orbitofrontal cortex. Nature Reviews Neuroscience, 17(8), 513.

Young, J. J., & Shapiro, M. L. (2011). Dynamic coding of goal-directed paths by orbital prefrontal cortex. Journal of Neuroscience, 31(16), 5989-6000.

Yamada, H., Louie, K., Tymula, A., and Glimcher, P.W. (2018). Free choice shapes normalized value signals in medial orbitofrontal cortex. Nature communications *9*, 162.

Zeithamova, D., de Araujo Sanchez, M. A., & Adke, A. (2017). Trial timing and pattern-information analyses of fMRI data. Neuroimage, 153, 221-231.